

SIMULATION OF GAUSSIAN RANDOM FIELDS ON SURFACES USING THE ISOGEOMETRIC FINITE ELEMENT METHOD

HELMUT HARBRECHT, FLORIAN SONDEREGGER,
AND REMO VON RICKENBACH

ABSTRACT. We are concerned with the fast simulation of random fields on closed surfaces in \mathbb{R}^3 which are generated by the (Whittle-) Matérn class of covariance functions. To this end, we solve the underlying fractional stochastic partial differential equation with additive white noise by using an isogeometric finite element method on the surface in combination with the Balakrishnan integral representation of the solution. The solution of the underlying linear system of equations is performed by means of a geometric multigrid method that naturally underlies the isogeometric approach. Numerical results are presented to demonstrate the approach.

1. INTRODUCTION

A commonly used category of statistical models is that of Gaussian processes, characterized by their mean and covariance structure. This involves the generation of correlated random data that follow a Gaussian distribution. In this article, we are interested in simulating such *Gaussian random fields* on surfaces of three-dimensional domains. They have been utilized in a variety of fields, for example in engineering, geostatistics, cosmological data analysis, and biomedical image analysis, compare [12, 26, 30] and the references therein.

To generate realizations of a specific Gaussian random field, we pursue with an approach that has its origin in computational spatial statistics [15, 16, 22, 23, 29]. This approach allows the efficient sampling for Gaussian random fields arising from the (Whittle-) Matérn class of covariance functions. As observed for \mathbb{R}^d in [33, 34], these covariance functions are given by

$$(1) \quad \mathcal{K}_\nu(\mathbf{x}, \mathbf{y}) := \frac{\sigma^2}{2^{\nu-1} \Gamma(\nu)} r^\nu K_\nu(r), \quad \text{where } r := \kappa \|\mathbf{x} - \mathbf{y}\|,$$

where ν is the smoothness parameter, determining the spatial (Sobolev) smoothness of the Matérn field, $\kappa > 0$ relates to the correlation length, Γ is the Riemannian gamma function and K_ν is the modified Bessel function of the second kind, see [25]

for example. The marginal variance σ^2 in (1) is given by

$$(2) \quad \sigma^2 = \frac{\Gamma(\nu)}{\Gamma(\nu + d/2)} (4\pi)^{-d/2} \kappa^{-2\nu}.$$

In the situation of a two-dimensional closed surface $\Gamma := \partial D$ of a given domain $D \subset \mathbb{R}^3$, we are in the situation of $d = 2$ and the distance $\|\mathbf{x} - \mathbf{y}\|$ in (1) should be the geodesic distance which is not easy to calculate on general surfaces. Therefore, we use the characterization of the random field as the solution of the following fractional partial differential equation with additive white noise:

$$(3) \quad (\kappa^2 I + \Delta_\Gamma)^\beta u = f \text{ on } \Gamma.$$

Herein, Δ_Γ denotes the Laplace-Beltrami operator on the given surface $\Gamma \subset \mathbb{R}^3$ while the fractional exponent β is related to the smoothness parameter ν in (1) via $\nu = 2\beta - 1$.

For $\beta \in (0, 1)$, the solution of the fractional partial differential equation can be computed by using the integral identity

$$(4) \quad (\kappa^2 I - \Delta_\Gamma)^\beta u = \frac{\sin(\pi\beta)}{\pi} \int_0^\infty t^{-\beta} (t + \kappa^2 - \Delta_\Gamma)^{-1} u \, dt,$$

which has been proven in [3]. In particular, this improper integral can be efficiently approximated by a sinc quadrature, see [24] for details. For $\beta > 1$, one splits $\beta = n + \beta'$ with the integer part $n \in \mathbb{N}$ being successively computable by solving for the Laplace-Beltrami operator and the fractional part $\beta' \in (0, 1)$ being computable by means of (4), compare [16]. However, for β' being close to 0 or 1, the convergence of the sinc quadrature becomes quite slow and we propose an improved splitting in Section 3.4.

The evaluation of the integrand in (4) at a sinc quadrature point amounts to solving a partial differential equation for the Laplace-Beltrami operator. In contrast to [6, 20, 21], we apply here the methodology from *isogeometric analysis* (IGA) to discretize this partial differential equation. This means that we employ a high-order or even exact representation of the underlying surface in terms of *non-uniform rational B-splines* (NURBS) in combination with a high-order spline based discretization of the partial differential equation. This enables to exploit the higher order smoothness of the underlying Gaussian random field when β is getting larger.

IGA has been introduced in [19] in order to incorporate simulation techniques into the design workflow of industrial development and thus allows to deal with surfaces in a straightforward manner. In addition, the naturally emerging sequence of nested approximation spaces can directly be employed in a multigrid method. Therefore,

the isogeometric finite element method is the method of choice for the problem at hand. In particular, we can rely on the C++-library `bemvel` which provides an implementation of the isogeometric boundary element method, naturally including isogeometric finite elements on surfaces, see [9, 10, 11] and also [18].

The rest of this article is organized as follows. Section 2 recapitulates the basic concepts from isogeometric analysis and introduces the discretization spaces that will be used later on. In Section 3, we introduce the discretization of the fractional boundary value problem under consideration and develop related solution algorithms. In Section 4, we present numerical results to validate the applicability and feasibility of the proposed approach for the simulation of Gaussian random fields arising from (Whittle-) Matérn covariance functions. Finally, in Section 5, we draw the article's conclusion.

2. ISOGEOMETRIC ANALYSIS

2.1. B-splines. We shall give a brief introduction to the basic concepts of isogeometric analysis, starting with the definition of the B-spline basis, followed by the description of the surface under consideration by using NURBS. The original definitions (or equivalent notions) and proofs, as well as basic algorithms, can be found in most of the standard spline and isogeometric literature [8, 19, 27, 31, 32].

Definition 2.1. *Let $0 \leq p \leq k$. We define a p -open knot vector as a set $\Xi := \{\xi_0, \dots, \xi_{n+p}\}$ such that*

$$\underbrace{\xi_0 = \dots = \xi_p}_{=0} < \xi_{p+1} < \dots < \xi_{k-1} < \underbrace{\xi_k = \dots = \xi_{k+p}}_{=1},$$

where k denotes the number of control points. The associated basis functions are given by $\{b_\ell^p\}_{\ell=0}^{k-1}$ for $p = 0$ as

$$b_\ell^0(x) = \begin{cases} 1, & \text{if } \xi_\ell \leq x < \xi_{\ell+1}, \\ 0, & \text{otherwise,} \end{cases}$$

and for $p > 0$ via the recursive relationship

$$b_\ell^p(x) = \frac{x - \xi_\ell}{\xi_{\ell+p} - \xi_\ell} b_\ell^{p-1}(x) + \frac{\xi_{\ell+p+1} - x}{\xi_{\ell+p+1} - \xi_{\ell+1}} b_{\ell+1}^{p-1}(x),$$

see Figure 1. A spline is then defined as a function

$$f(x) = \sum_{0 \leq \ell < k} p_\ell b_\ell^p(x),$$

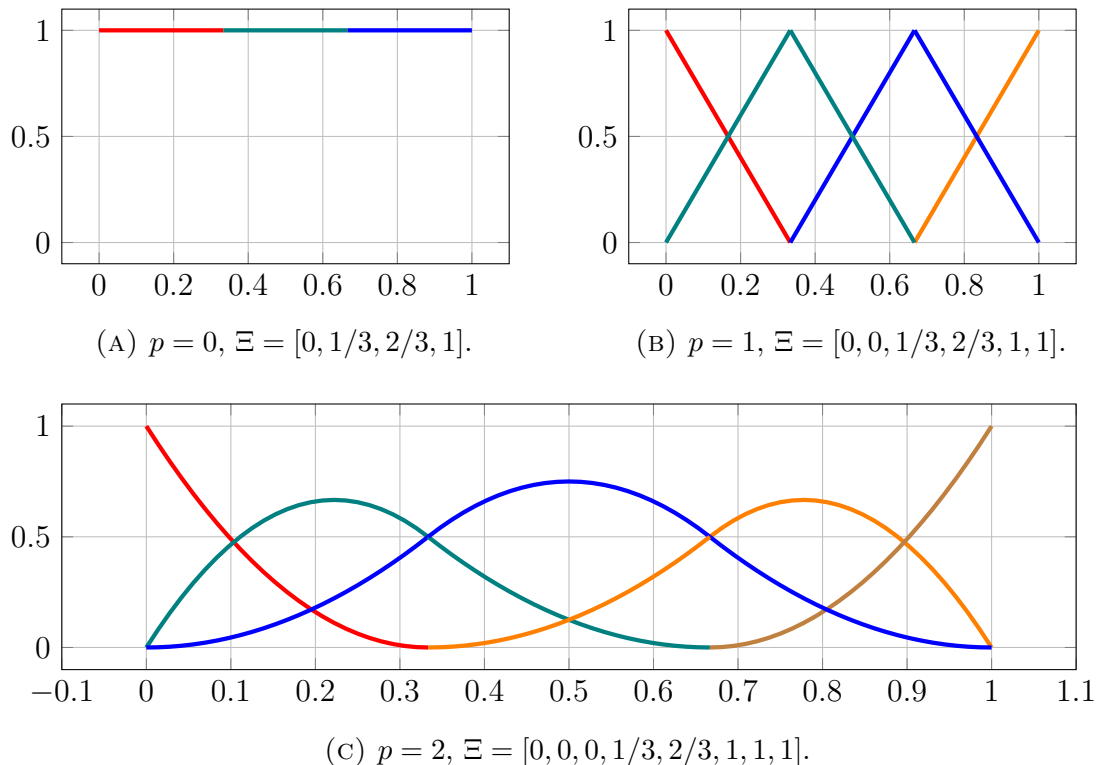


FIGURE 1. B-spline bases for $p = 0, 1, 2$ and open knot vectors with interior knots $1/3$ and $2/3$.

where $\{p_\ell\}_{\ell=0}^{k-1} \subset \mathbb{R}$ denotes the set of control points. If one sets $\{p_\ell\}_{\ell=0}^{k-1} \subset \mathbb{R}^d$ with $d \geq 2$, then f will be called a spline curve.

Having the spline functions at hand, we can introduce the spline spaces which serve as fundament for the definition of the ansatz and test spaces of the finite element method on the surface.

Definition 2.2. Let Ξ be a p -open knot vector containing $k + p + 1$ elements. We define the spline space $S_p(\Xi)$ as the space spanned by $\{b_\ell^p\}_{\ell=0}^{k-1}$.

Finally, we should consider the relationship between the spline spaces and the underlying mesh relative to a specific mesh size.

Definition 2.3. For a knot vector Ξ , we define the mesh size h to be the maximal distance

$$(5) \quad h := \max_{\ell=p}^k h_\ell, \quad \text{where} \quad h_\ell := \xi_{\ell+1} - \xi_\ell,$$

between neighbouring knots. We call the knot vector quasi uniform, when there exists a constant $\theta > 0$ such that for all ℓ the ratio h_ℓ/h satisfies $h_\ell/h \geq \theta$.

B-splines on two-dimensional domains are constructed by means of the tensor product

$$(6) \quad f(x, y) = \sum_{\ell_1=0}^{k_1-1} \sum_{\ell_2=0}^{k_2-1} \mathbf{p}_{\ell_1, \ell_2} b_{\ell_1}^{p_1}(x) b_{\ell_2}^{p_2}(y)$$

with control points $\mathbf{p}_{\ell_1, \ell_2} \in \mathbb{R}^d$. This allows the definition *tensor product spline spaces* in accordance with

$$S_{p_1, p_2}(\Xi_1, \Xi_2).$$

Throughout this article, we will reserve the letter h for the mesh size (5). All knot vectors will be assumed to be quasi uniform, such that the usual spline theory is applicable, see [5, 27, 31] for example.

2.2. Isogeometric representation of the surface. We assume that the boundary Γ of the domain under consideration is closed and Lipschitz continuous. For the remainder of this article, we assume that it is given patchwise as $\Gamma = \bigcup_{m=1}^n \Gamma_m$, i.e. that it is induced by smooth diffeomorphisms

$$(7) \quad \mathbf{F}_m: \square = [0, 1]^2 \rightarrow \Gamma_m \subset \mathbb{R}^3.$$

In the spirit of isogeometric analysis, these mappings are given by NURBS mappings, i.e. by

$$\mathbf{F}_m(x, y) := \sum_{\ell_1=0}^{k_1-1} \sum_{\ell_2=0}^{k_2-1} \frac{c_{\ell_1, \ell_2} b_{\ell_1}^{p_1}(x) b_{\ell_2}^{p_2}(y) w_{\ell_1, \ell_2}}{\sum_{i_1=0}^{k_1-1} \sum_{i_2=0}^{k_2-1} b_{i_1}^{p_1}(x) b_{i_2}^{p_2}(y)} w_{i_1, i_2}$$

with control points $c_{\ell_1, \ell_2} \in \mathbb{R}^3$ and weights $w_{i_1, i_2} > 0$. We will moreover require that, for any interface $D = \Gamma_{m_1} \cap \Gamma_{m_2} \neq \emptyset$, the NURBS mappings coincide, i.e. that, up to rotation of the reference domain, one finds $\mathbf{F}_{m_1}(\cdot, 1) \equiv \mathbf{F}_{m_2}(\cdot, 0)$.

2.3. Finite element spaces. The mappings of (7) give rise to the transformations

$$\iota_m(f) := f \circ \mathbf{F}_m,$$

which are employed to define discrete spaces patchwise, by mapping the space of tensor product B-splines as in (6) with

$$\Xi_{j,p} := \left\{ \underbrace{0, \dots, 0}_{p+1 \text{ times}}, 2^{-j}, \dots, 1 - 2^{-j}, \underbrace{1, \dots, 1}_{p+1 \text{ times}} \right\}$$

to the geometry. Here, the variable j denotes the level of uniform refinement.

Let us first introduce the space of patchwise continuous B-splines on Γ by

$$\mathbb{S}_{j,p}^2(\Gamma) := \left\{ f \in L^2(\Gamma) : f|_{\Gamma_m} \equiv \iota_m^{-1}(g) \text{ for some } g \in S_{p,p}(\Xi_{j,p}, \Xi_{j,p}) \right\},$$

It is of dimension $n \cdot (2^j + p)^2$, where n denotes the number of patches involved in the description of the geometry. For our purpose of discretizing the Laplace-Beltrami operator, we however require globally continuous B-splines and hence the subspace

$$(8) \quad \mathbb{S}_{j,p}^0(\Gamma) := \left\{ f \in C(\Gamma) : f|_{\Gamma_m} \equiv \iota_m^{-1}(g) \right. \\ \left. \text{for some } g \in S_{p,p}(\Xi_{j,p}, \Xi_{j,p}) \right\} \subset \mathbb{S}_{j,p}^2(\Gamma).$$

This space will serve as ansatz and test space in the Galerkin method to solve the underlying boundary value problem. It especially provides the approximation property

$$(9) \quad \inf_{u_j \in \mathbb{S}_{j,p}^0(\Gamma)} \|u - u_j\|_{L^2(\Gamma)} \lesssim 2^{-j(p+1)} \|u\|_{H^{p+1}(\Gamma)}$$

provided that there holds $u \in H^{p+1}(\Gamma)$.

3. DISCRETIZATION

3.1. Galerkin method. The evaluation of the integral (4) relies on the numerical solution of the partial differential equation

$$(10) \quad (t + \Delta_\Gamma)u = f \text{ on } \Gamma$$

for given $t \in \mathbb{C}$ and some right-hand side f . To derive the variational formulation of this problem, we let

$$\langle u, v \rangle_\Gamma = \int_\Gamma u(\mathbf{x})v(\mathbf{x}) \, d\sigma$$

denote the surface integral over Γ . Then, we the variational formulation reads:

$$(11) \quad \text{Find } u \in H^1(\Gamma) \text{ such that} \\ t\langle u, v \rangle_\Gamma + \langle \nabla_\Gamma u, \nabla_\Gamma v \rangle_\Gamma = \langle f, v \rangle_\Gamma \quad \text{for all } v \in H^1(\Gamma).$$

Here, $\nabla_\Gamma u$ denotes the surface gradient of the function u . Given a function $w : \mathbb{R}^3 \rightarrow \mathbb{R}$, it is defined in accordance with

$$\nabla_\Gamma w = \nabla w - \frac{\partial w}{\partial \mathbf{n}} \mathbf{n}.$$

For the discretization of the variational formulation, we replace the energy space $H^1(\Gamma)$ by the spline space $\mathbb{S}_{j,p}^0(\Gamma)$. Thus, the discrete variational formulation for (11) reads

$$\text{Find } u_h \in \mathbb{S}_{j,p}^0(\Gamma) \text{ such that} \\ t\langle u_h, v_h \rangle_\Gamma + \langle \nabla_\Gamma u_h, \nabla_\Gamma v_h \rangle_\Gamma = \langle f, v_h \rangle_\Gamma \quad \text{for all } v_h \in \mathbb{S}_{j,p}^0(\Gamma),$$

where $u_h \approx u$ is the Galerkin approximation of the solution u to (10). Setting $N := \dim(S_{j,p}^0(\Gamma))$ and choosing a basis

$$\mathbb{S}_{j,p}^0(\Gamma) = \text{span}\{\varphi_1, \dots, \varphi_N\}$$

of the underlying ansatz space leads to the system of linear equations

$$(12) \quad (\kappa^2 \mathbf{M} + \mathbf{S})\mathbf{u} = \mathbf{f}$$

with the mass matrix \mathbf{M} , stiffness matrix \mathbf{S} , and right-hand side \mathbf{f} given by

$$\mathbf{M} = [\langle \varphi_j, \varphi_i \rangle_\Gamma]_{i,j=1}^N, \quad \mathbf{S} = [\langle \nabla_\Gamma \varphi_j, \nabla_\Gamma \varphi_i \rangle_\Gamma]_{i,j=1}^N, \quad \mathbf{f} = [\langle f, \varphi_i \rangle_\Gamma]_{i=0}^N,$$

and \mathbf{u} being the coefficient vector of u_h .

3.2. Reformulation on the reference domain. Due to the isogeometric representations of the geometry, the bilinear forms for the computation of the matrix entries can entirely be pulled back to the reference domain [14]. We define the *first fundamental tensor of differential geometry* of a mapping \mathbf{F}_m for $\hat{\mathbf{x}} = (x, y) \in [0, 1]^2$ by

$$\mathbf{K}_m(\hat{\mathbf{x}}) := \begin{bmatrix} \partial_x \mathbf{F}_m(\hat{\mathbf{x}})^\top \partial_x \mathbf{F}_m(\hat{\mathbf{x}}) & \partial_x \mathbf{F}_m(\hat{\mathbf{x}})^\top \partial_y \mathbf{F}_m(\hat{\mathbf{x}}) \\ \partial_y \mathbf{F}_m(\hat{\mathbf{x}})^\top \partial_x \mathbf{F}_m(\hat{\mathbf{x}}) & \partial_y \mathbf{F}_m(\hat{\mathbf{x}})^\top \partial_y \mathbf{F}_m(\hat{\mathbf{x}}) \end{bmatrix}.$$

Then, the associated *surface measure* can be expressed by

$$a_m(\hat{\mathbf{x}}) := \|\partial_x \mathbf{F}_m(\hat{\mathbf{x}}) \times \partial_y \mathbf{F}_m(\hat{\mathbf{x}})\|_2 = \sqrt{\det \mathbf{K}_m(\hat{\mathbf{x}})}.$$

Thus, the bilinear form related to the mass matrix can be recast as

$$(13) \quad \begin{aligned} \langle u, v \rangle_\Gamma &= \sum_{m=1}^n \int_{[0,1]^2} u(\mathbf{F}_m(\hat{\mathbf{x}})) v(\mathbf{F}_m(\hat{\mathbf{x}})) a_m(\hat{\mathbf{x}}) \, d\hat{\mathbf{x}} \\ &= \sum_{m=1}^n \int_{[0,1]^2} u_m(\hat{\mathbf{x}}) v_m(\hat{\mathbf{x}}) a_m(\hat{\mathbf{x}}) \, d\hat{\mathbf{x}} \end{aligned}$$

with the pull-back

$$u_m(\hat{\mathbf{x}}) = \iota_m(u)(\hat{\mathbf{x}}), \quad v_m(\hat{\mathbf{y}}) = \iota_m(v)(\hat{\mathbf{y}})$$

of the ansatz and test functions.

In order to compute the stiffness matrix, we note that the surface gradient of a function u defined on the patch Γ_m is given by

$$\nabla_\Gamma u(\mathbf{F}_m(\hat{\mathbf{x}})) = \begin{bmatrix} \partial_x \mathbf{F}_m(\hat{\mathbf{x}}) & \partial_y \mathbf{F}_m(\hat{\mathbf{x}}) \end{bmatrix} \mathbf{K}_m^{-1}(\hat{\mathbf{x}}) \begin{bmatrix} \partial_x u_m(\hat{\mathbf{x}}) \\ \partial_y u_m(\hat{\mathbf{x}}) \end{bmatrix}.$$

Hence, we arrive at the identity

$$(14) \quad \langle \nabla_{\Gamma} u, \nabla_{\Gamma} v \rangle_{\Gamma} = \sum_{m=1}^n \int_{[0,1]^2} \left[\partial_x u_m(\hat{\mathbf{x}}), \partial_y u_m(\hat{\mathbf{x}}) \right] \mathbf{K}_m^{-1}(\hat{\mathbf{x}}) \begin{bmatrix} \partial_x v_m(\hat{\mathbf{x}}) \\ \partial_y v_m(\hat{\mathbf{x}}) \end{bmatrix} a_m(\hat{\mathbf{x}}) d\hat{\mathbf{x}}.$$

Thus, the entries of the mass matrix and the stiffness matrix can be computed by means of (13) and (14) using appropriately chosen quadrature formulae that provide sufficient accuracy.

3.3. Computing the right-hand side. The right-hand side f in (3) corresponds to white noise. The associated discrete right-hand side \mathbf{f} is thus normally distributed in accordance with $\mathbf{f} \sim \mathcal{N}(\mathbf{0}, \mathbf{M})$, compare [16]. The simulation of the desired Gaussian random field requires therefore the application of the matrix square root of \mathbf{M} , as a specific realization is generated by $\mathbf{f} = \sqrt{\mathbf{M}}\mathbf{y}$ with \mathbf{y} being a sequence of i.i.d. $\mathcal{N}(0, 1)$ -distributed random variables.

The computation of the square root $\sqrt{\mathbf{M}}$ to the mass matrix \mathbf{M} can be carried out in accordance with [13, Eq. (4.4) and comments below]: Let $0 < m < \min \lambda(\mathbf{M})$ be a lower bound for smallest eigenvalue of the mass matrix \mathbf{M} and $M > \max \lambda(\mathbf{M})$ be an upper bound for its largest eigenvalue. Then, for some $\hat{K} \in \mathbb{N}$ and $\varkappa_{\mathbf{M}} := M/m$, we compute

$$(15) \quad \mathbf{f} = \sqrt{\mathbf{M}}\mathbf{y} \approx \frac{2E\sqrt{m}}{\pi\hat{K}}\mathbf{M} \sum_{k=1}^{\hat{K}} \frac{\operatorname{dn}(t_k|1 - \varkappa_{\mathbf{M}}^{-1})}{\operatorname{cn}^2(t_k|1 - \varkappa_{\mathbf{M}}^{-1})} (\mathbf{M} + w_k^2\mathbf{I})^{-1}\mathbf{y}.$$

Here, sn , cn and dn are the Jacobian elliptic functions (see [1, Chpt. 16]), E is the complete elliptic integral of the second kind associated with the parameter $\varkappa_{\mathbf{M}}^{-1}$ (see [1, Chpt. 17]), and

$$w_k := \sqrt{m} \frac{\operatorname{sn}(t_k|1 - \varkappa_{\mathbf{M}}^{-1})}{\operatorname{cn}(t_k|1 - \varkappa_{\mathbf{M}}^{-1})}, \quad t_k := \frac{(k - \frac{1}{2})E}{\hat{K}}, \quad k \in \{1, \dots, \hat{K}\}.$$

Note that the computation of the approximation (15) requires only the repeated solution of (well-conditioned) linear systems of equations involving the mass matrix. The convergence towards the exact result $\sqrt{\mathbf{M}}\mathbf{y}$ is exponential in the parameter \hat{K} , compare [13, Thm 4.1].

We remark that white noise satisfies $f \in L_{\mathbb{P}}^2(\Omega) \otimes H^{-r}(\Gamma)$ for any $r > 1$, see [4, 16] for example. Hence, the Gaussian random field u given by (3) satisfies $u \in L_{\mathbb{P}}^2(\Omega) \otimes H^{2\beta-r}(\Gamma)$. If $\beta > \frac{3}{2}$, linear finite elements are no more optimal and higher order ansatz functions pay off. More precisely, we have the error estimate

$$\|u - u_j\|_{L_{\mathbb{P}}^2(\Omega) \otimes L^2(\Gamma)} \lesssim 2^{-j \min\{p+1, 2\beta-1-\delta\}} \quad \text{for any } \delta > 0$$

for the mean-square error of the approximate Gaussian random field u_j provided that the surface Γ is smooth enough, compare [16].

3.4. Solving equations with fractional powers. Once we have the stiffness matrix \mathbf{S} , the mass matrix \mathbf{M} , and the right-hand side \mathbf{f} at hand, we shall consider the discretization of the equation (3). If $\beta = 1$, this is not a problem, as we can solve

$$(\kappa^2 \mathbf{M} + \mathbf{S})\mathbf{u} = \mathbf{f}$$

in a straightforward manner. If $\beta \in \mathbb{N}$ with $\beta \geq 2$, we successively solve equation (10) just β times, i.e.

$$(\kappa^2 \mathbf{M} + \mathbf{S})\mathbf{w}_1 = \mathbf{f} \quad \text{and} \quad (\kappa^2 \mathbf{M} + \mathbf{S})\mathbf{w}_k = \mathbf{M}\mathbf{w}_{k-1} \quad \text{for } k = 2, \dots, \beta,$$

to get the approximation $\mathbf{u} := \mathbf{w}_\beta$. If $\beta \notin \mathbb{N}$, we can follow [16] and split β into its integer part and the remainder $\in (0, 1)$. We hence can assume without loss of generality that $\beta \in (0, 1)$ since the integer part can be treated as described above.

The solution of (3) for $\beta \in (0, 1)$ will be performed as proposed in [6, 16] by using the representation (4). We choose $K \in \mathbb{N}$ and compute

$$(16) \quad \mathbf{u} \approx \mathbf{u}_K = \frac{2 \sin(\pi\beta)}{\sqrt{K}\pi} \sum_{k=-K}^K e^{2\beta t_k} (\mathbf{I} + e^{2t_k} \mathbf{A})^{-1} \mathbf{f}$$

with quadrature points $t_k = k/\sqrt{K}$ and $\mathbf{A} = \kappa^2 \mathbf{M} + \mathbf{S}$. As shown in [16, Lemma 2.3], we obtain exponential convergence with respect to \sqrt{K} according to

$$(17) \quad \|\mathbf{u} - \mathbf{u}_K\| \lesssim e^{-2 \min\{\beta, 1-\beta\} \sqrt{K}} \|\mathbf{f}\|,$$

where the constant involved does not depend on β .

The convergence rate (17) of the sinc quadrature depends crucially on β . It is best for $\beta = 1/2$ and gets significantly worse when β is close to 0 or 1. Thus, we propose the following modification compared to [16] if β is close to an integer n :

- If $\beta = n + \beta'$ with $\beta' \in (0, 1/3)$, we split $\beta = n - 1 + 2\beta''$ with $\beta'' = (\beta'+1)/2 \in (1/2, 2/3)$ instead of using the integer and fractional parts of β .
- If $\beta = n + \beta'$ with $\beta' \in (2/3, 1)$, we split $\beta = n + 2\beta''$ with $\beta'' = \beta'/2 \in (1/3, 1/2)$ instead of using the integer and fractional parts of β .

One readily verifies from (17) that the convergence for β'' is in both cases faster than for β' . Although we have to apply (16) twice in this new approach, we obtain improved computation times in comparison to the original approach of [16] as we demonstrate in Section 4.

3.5. Preconditioning. In isogeometric analysis, we naturally obtain a sequence of nested ansatz spaces as the step size h tends to zero. This allows for geometric multigrid techniques for the solution of the linear system of equations resulting from the discretization of the variational formulation (11). In our numerical experiments, we consider both, the multiplicative multigrid method by means of the V-cycle and the additive multigrid method by means of the BPX preconditioner. These methods have been introduced in the context isogeometric analysis in [7, 17]. Thus, we obtain a linear cost-complexity rate for the computation of the numerical approximation to (11). Nonetheless, a polynomial dependency of the complexity on the polynomial degree p remains.

4. NUMERICAL EXPERIMENTS

4.1. Results for the sphere. The first surface we consider is the unit sphere $\mathbb{S}^2 = \{(x, y, z) \in \mathbb{R}^3 : x^2 + y^2 + z^2 = 1\}$, which is parametrized by six patches as seen in Figure 2. In order to test our implementation, we use the spherical harmonics $Y_{\ell,m}$, as they are known to be the eigenfunctions of the Laplace-Beltrami operator on the unit sphere, see [2] for example. In our experiments, we especially study the influence of the polynomial degree p and the refinement level j on the proposed algorithms.

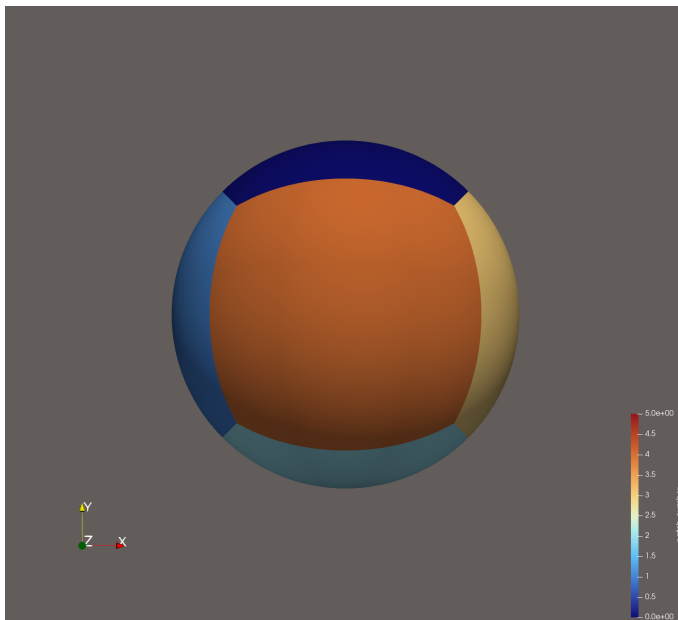


FIGURE 2. The unit sphere, consisting of 6 patches.

4.1.1. *Rate of convergence.* The isogeometric finite element implementation of the Laplace-Beltrami operator is tested on the unit sphere with the problem

$$(18) \quad (\kappa^2 - \Delta_\Gamma)u = Y_{1,-1} \quad \text{on } \Gamma = \mathbb{S}^2,$$

which has the analytical solution

$$u = \frac{1}{2 + \kappa^2} Y_{1,-1}.$$

We choose $\kappa = 1$ as a convenient value, but the choice of κ does not impact the results. We discretize the equation (18) as described in the previous sections and solve the resulting linear system of equations by using Eigen's conjugate gradient method with tolerance $\varepsilon = 10^{-12}$ for different refinement levels j and corresponding mesh sizes $h_j \sim 2^{-j}$. The errors obtained for different polynomial degrees $1 \leq p \leq 5$ of our ansatz space are reported in Figure 3. As one figures out thereof, the convergence rates observed match the theoretical rates from (9):

$$\|u - u_j\|_{L^2(\mathbb{S}^2)} \lesssim 2^{-j(p+1)} \|u\|_{H^{p+1}(\mathbb{S}^2)}.$$

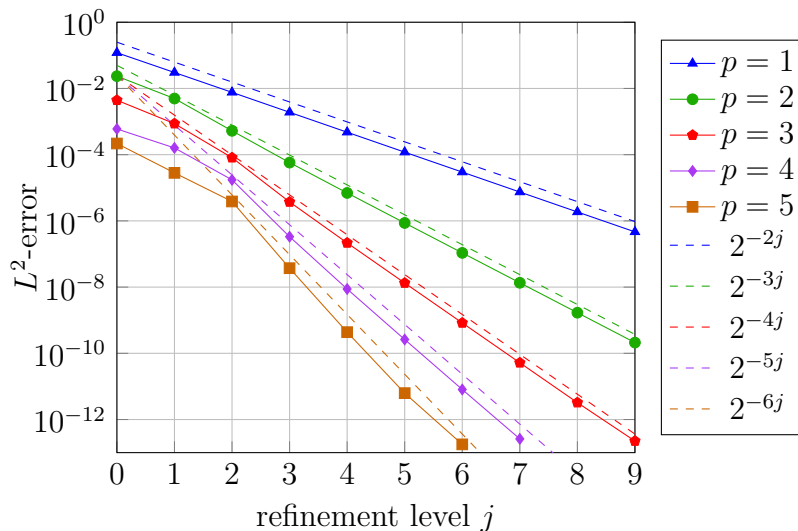


FIGURE 3. Convergence rate of the approximate solution to (18) in dependence of the refinement level j and the polynomial degree p .

4.1.2. *Preconditioning.* We shall next study the preconditioning of the linear system of equations which arises from the isogeometric finite element discretization of the boundary value problem (18). To this end, we apply the conjugate gradient method, which we precondition by the BPX-preconditioner with either a diagonal scaling on each level (“BPX-diag”) or an SSOR preconditioning on each level (“BPX-SSOR”),

cf. [7] for the details. The computational complexity is then linear in the number of degrees of freedom if the system of linear equations are solved with fixed accuracy, but it depends on the polynomial degree p . This has already been reported in [7] and matches the theory since the spectral condition number of the preconditioned system matrix is independent of the mesh size h_j but depends on p . Indeed, we observe a basically linear increase of the runtimes in Figure 4 in the number of degrees of freedom for fixed polynomial degree p . As it can be expected, the BPX-SSOR variant takes less iterations per refinement level j , compare Table 1. However, it is also computationally more expensive. Hence, we barely notice a difference in the runtimes in practice between both variants of the BPX-preconditioner.

j	BPX with diagonal scaling					BPX with SSOR				
	$p = 1$	$p = 2$	$p = 3$	$p = 4$	$p = 5$	$p = 1$	$p = 2$	$p = 3$	$p = 4$	$p = 5$
0	1	2	4	9	15	4	8	19	36	70
1	2	4	9	15	39	11	16	29	52	105
2	8	11	24	34	76	18	21	34	64	115
3	17	28	62	93	177	21	25	38	68	122
4	21	39	87	163	343	23	27	42	73	135
5	24	44	99	204	423	26	29	44	77	141
6	27	49	108	223	462	28	31	47	81	147
7	29	53	116	238	494	29	33	49	85	152
8	30	56	124	253	525	31	34	51	88	157
9	32	59	130	264	548	32	35	53	91	161

TABLE 1. Number of iterations of the preconditioned conjugate gradient with BPX-preconditioning in case of a diagonal scaling on each level and in case of an SSOR preconditioning on each level.

We like to mention that we also tested a multiplicative multigrid using the V -cycle. It turned out to be less robust with respect to higher polynomial degree p and with respect to the geometry. In all the test cases we considered, the conjugate gradient method in combination with the BPX-preconditioner was more efficient.

4.1.3. *Sinc quadrature.* We next consider the fractional problem

$$(\kappa^2 - \Delta_\Gamma)^\beta u = Y_{1,-1} \quad \text{on } \Gamma = \mathbb{S}^2$$

with analytical solution

$$u = \left(\frac{1}{2 + \kappa^2} \right)^\beta Y_{1,-1}.$$

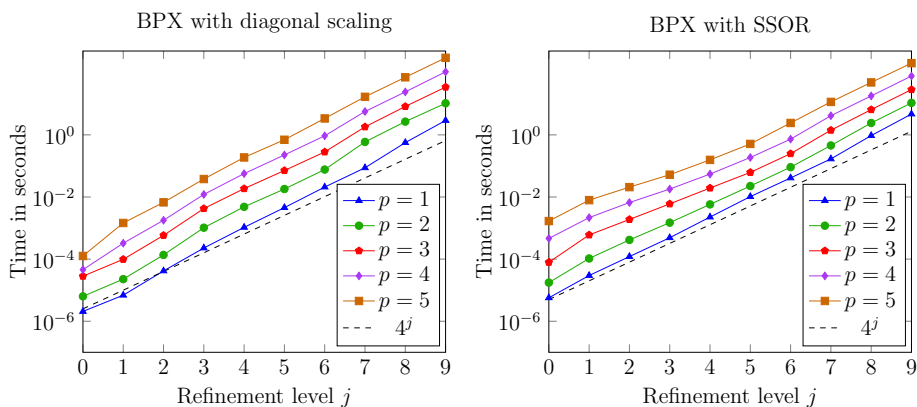


FIGURE 4. Runtime of the conjugate gradient with BPX-preconditioning in case of a diagonal scaling on each level (left) and in case of an SSOR preconditioning on each level (right).

We solve this fractional problem by using the sinc quadrature for $p = 3$ and $j = 5$ (where we can expect an discretization error of about 10^{-8}) and the number of quadrature points K ranging from 2 to 500. The convergence rate we observe matches the predicted rate of $\exp(C_\beta \sqrt{K})$, where $C_\beta = -2 \min\{\beta, 1 - \beta\}$, compare (17). It should also be noted that the multiplicative constants hidden in the error rates seem to be independent of β , as is important for our new proposed method of solving (3) for fractional β being close to an integer.

We shall next compare in Figure 6 the two methods for approximating $(\kappa^2 + \Delta_\Gamma)^{-\beta} f$ for $1 < \beta \leq 4/3$. We expect that the old method, where we split β into 1 and $\beta - 1$ should be faster for all $\beta \in (4/3, 3/2)$, whereas the new method, where we split β into $\beta/2$ twice, is faster for $\beta \in (1, 4/3)$. We apply both methods with the same total number of quadrature nodes used, taking into account that we have to apply the quadrature twice for the new method. Indeed, as seen in Figure 6, the new method is faster for $\beta \leq 5/4$ which is a slightly smaller range than predicted.

4.1.4. *Matrix square root.* We test the convergence of the expansion (15) for approximating the multiplication of a given vector \mathbf{y} with the square root of the mass matrix \mathbf{M} by applying it twice to a random vector \mathbf{y} and then calculating the error

$$\left\| \mathbf{M}\mathbf{y} - \mathbf{M}_K^\vee \mathbf{M}_K^\vee \mathbf{y} \right\|.$$

This gives an error which is of the same order of magnitude as

$$\left\| \sqrt{\mathbf{M}}\mathbf{y} - \mathbf{M}_K^\vee \mathbf{y} \right\|$$

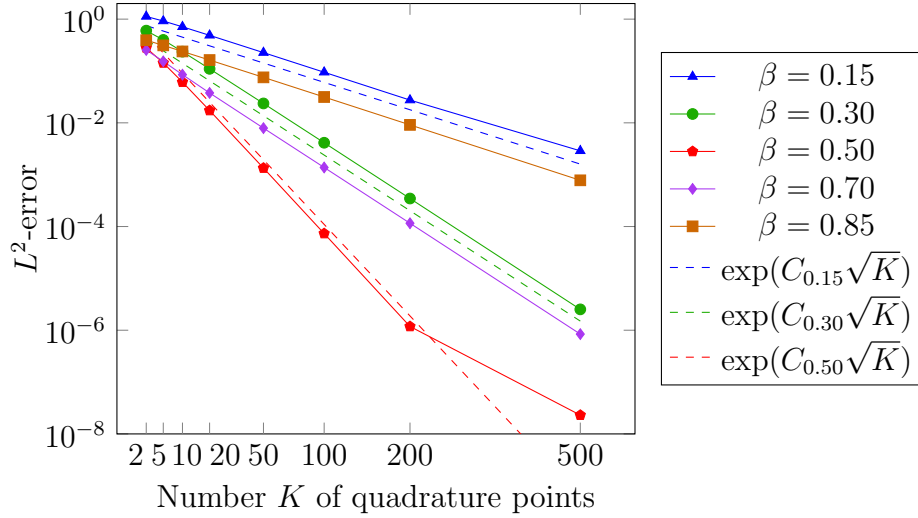


FIGURE 5. Convergence of the sinc quadrature with respect to the number K of quadrature points for fixed level of refinement $j = 6$ and polynomial degree $p = 3$.

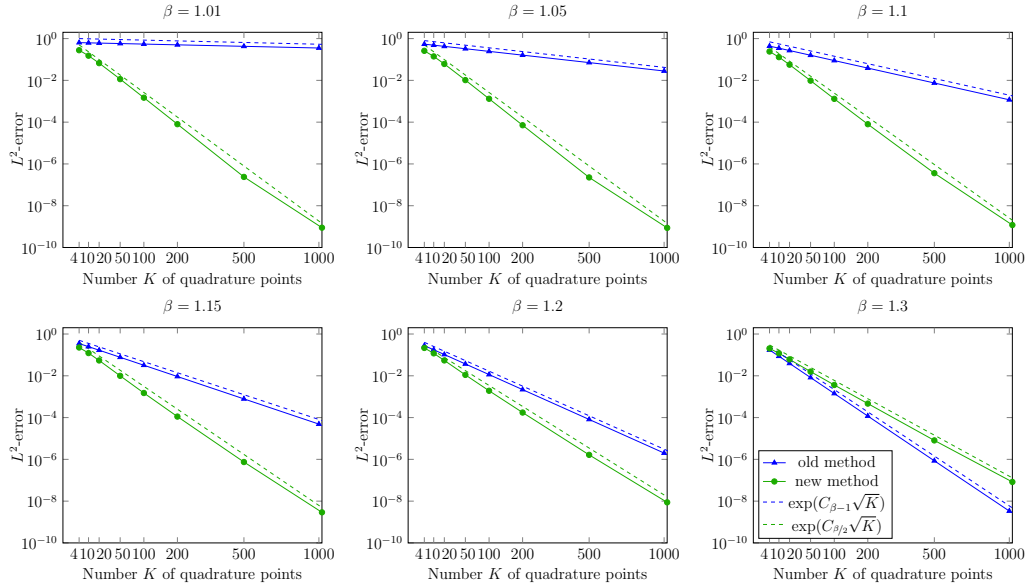


FIGURE 6. Comparison of both proposed methods for solving the fractional operator for certain values of $\beta \in (1, 1.3]$. When $\beta \in (1, 5/4)$, then solving twice for $\beta/2$ is superior (green graphs) to solving first for $\beta' = 1$ and then for $\beta' = \beta - 1$ (blue graphs).

without needing to calculate the exact matrix square root. Note that the quantity \varkappa_M appearing in (15) has been estimated by computing the largest and smallest eigenvalue of M by 20 steps of the (inverse) power method.

We see in Figure 7 that the convergence of the approximation towards the desired solution is indeed exponential in the parameter \hat{K} , with constants depending on the condition number of the mass matrix (left plot in Figure 7), thus on the polynomial degree p , but not on the refinement level j (right plot in Figure 7). This results in linear complexity in the number of degrees of freedom for a fixed value of \hat{K} and thus in a complexity $\mathcal{O}(N \log N)$ for the desired accuracy matching the discretization error of the ansatz space.

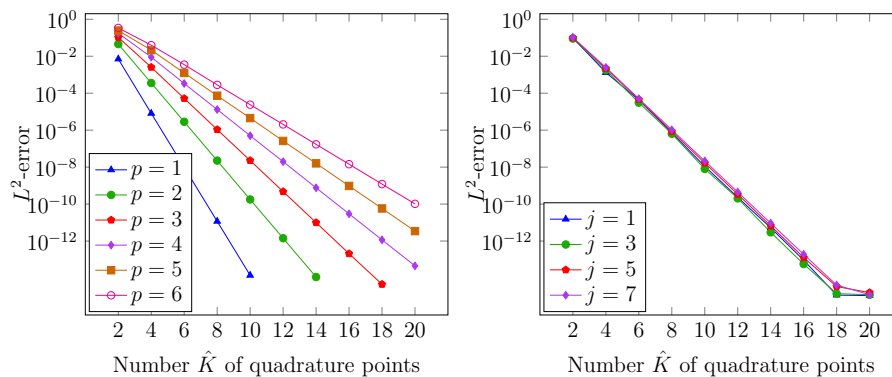


FIGURE 7. Comparison between the convergence rates of the matrix square root with respect to the number \hat{K} of terms in (15) for different polynomial degrees p and fixed level $j = 6$ (left) and different refinement levels j and fixed polynomial degree $p = 3$ (right).

Gaussian random field simulation. Last but not least, we present some realizations of Gaussian Whittle-Matérn fields for different parameters β and κ . As can be seen in Figure 8, the parameter β determines the smoothness of the random field while the parameter κ is inversely proportional to the correlation length of the random field.

4.2. Drilled cube and Stanford bunny. Finally, we demonstrate that our approach applies also to other, especially nontrivial surface representations: we turn our attention to a drilled cube and to the famous Stanford bunny found in Figure 9. The drilled cube is parametrized by 48 quadrangular patches while the Stanford bunny is parametrized by 179 patches. The parametrization of the Stanford bunny has been introduced in [18] and is based on the quadrangulation from [28]. We refer to these references for further details about the generation of the surface representation.

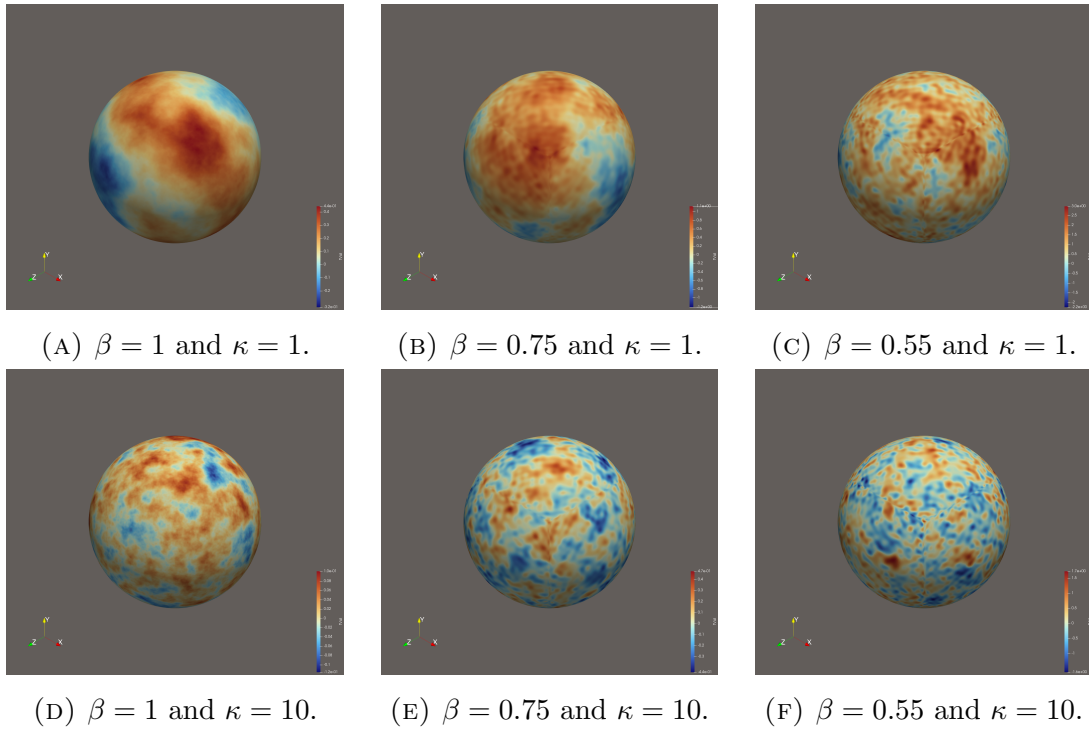


FIGURE 8. Whittle-Matérn Gaussian random fields on the unit sphere for different parameters of the fractional index β and the correlation length κ .

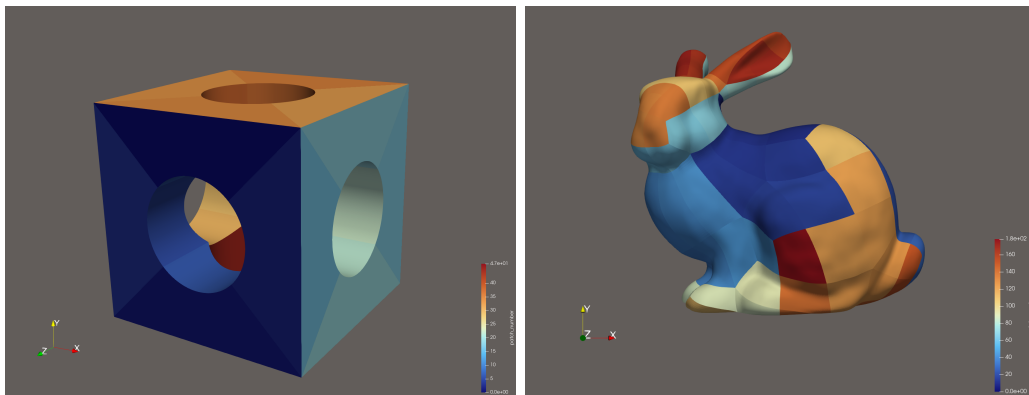


FIGURE 9. Parametrizations of a drilled cube (left) by 48 quadrangular patches and of the Stanford bunny (right) by 179 quadrangular patches.

Although the surface of the Stanford bunny is much more complex in comparison with the unit sphere, all the algorithms behave essentially the same as on the unit sphere, such that we refrain from presenting detailed results here. In particular,

the performance of the V-cycle multigrid is rather poor in case of the Stanford bunny since we need a lot of pre- and post-smoothing steps to ensure convergence. In contrast, the preconditioned conjugate gradient method converges well for all polynomial degrees $1 \leq p \leq 5$ in case of both BPX-variants. Table 2 reports the results for the Stanford bunny, which are quite similar to that obtained for the unit sphere.

j	BPX with diagonal scaling					BPX with SSOR				
	$p = 1$	$p = 2$	$p = 3$	$p = 4$	$p = 5$	$p = 1$	$p = 2$	$p = 3$	$p = 4$	$p = 5$
0	64	89	143	261	531	27	35	47	73	150
1	79	123	190	335	751	40	49	61	95	183
2	100	144	216	347	754	53	60	72	102	198
3	132	170	244	376	690	67	69	85	116	178
4	178	203	278	425	708	85	82	98	138	198
5	230	236	322	485	814	104	94	115	163	245

TABLE 2. Number of iterations of the preconditioned conjugate gradient with BPX-preconditioning in case of a diagonal scaling on each level and in case of an SSOR preconditioning on each level.

On both surfaces under consideration, we simulate Gaussian random fields generated by Whittle-Matérn covariance functions with the same set of parameters as for the unit sphere. Visualizations of these Whittle-Matérn Gaussian random fields can be found in Figure 10 for the drilled cube and in Figure 11 for the Stanford bunny. The level of refinement has been set to $j = 5$ and the polynomial degree to $p = 2$.

5. CONCLUSION

In the present article, we proposed the application of the isogeometric finite element method for the fast simulation of Gaussian random fields on surfaces which are generated by the (Whittle-) Matérn class of covariance functions. The isogeometric finite element method is able to compute realizations of the desired Gaussian random field in essentially linear overall complexity. This means the complexity is linear in the number of degrees of freedom except for polylogarithmic terms.

Compared to previous approaches from [6, 20, 21] which are based on planar or curved *linear* surface finite elements, the isogeometric finite element method enables higher rates of convergences in case of Gaussian random fields of sufficiently high smoothness since the polynomial degree p of the ansatz spaces can also be chosen larger than $p = 1$. Numerical results have been reported which validate the

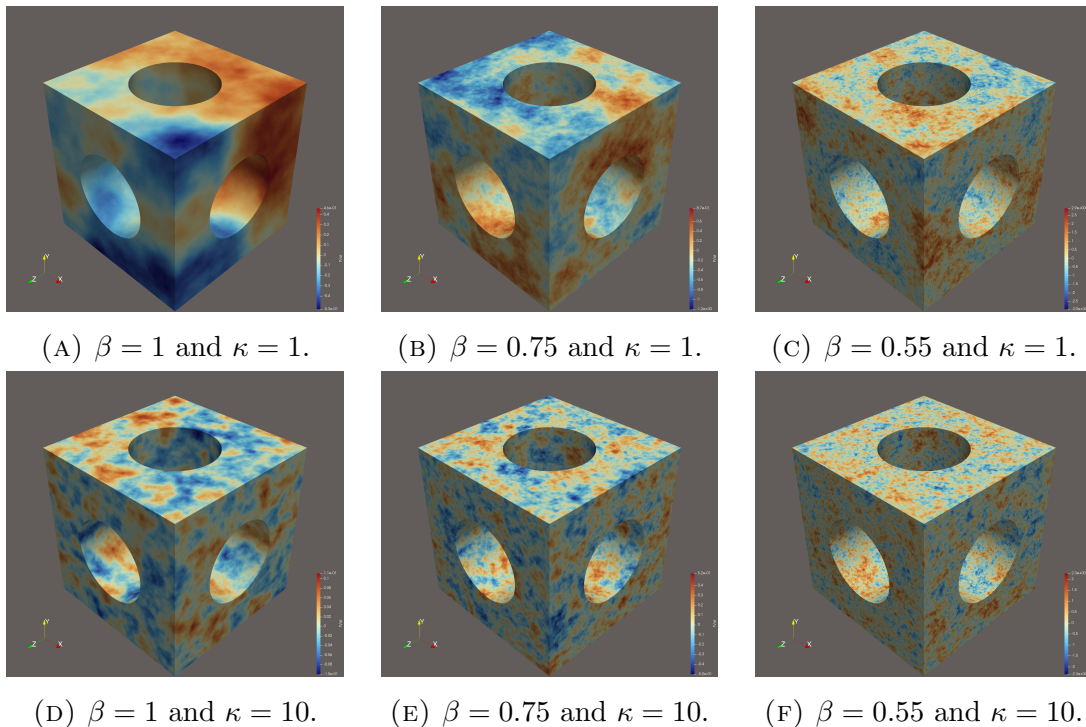


FIGURE 10. Whittle-Matérn Gaussian random fields on drilled cube for different parameters of the fractional index β and the correlation length κ .

applicability and feasibility of the isogeometric approach also on complicated surfaces.

Although we restricted ourselves to stationary Gaussian random fields being defined on two-dimensional surfaces, the extension of the present methodology to nonstationary Gaussian random fields is easily possible, see e.g. [21, 23] for the details.

REFERENCES

- [1] M. Abramowitz and I.A. Stegun. *Handbook of Mathematical Functions with Formulas, Graphs, and Mathematical Tables*, volume 55 of *National Bureau of Standards Applied Mathematics Series*. For sale by the Superintendent of Documents, U.S. Government Printing Office, Washington, D.C., 1964.
- [2] K. Atkinson and W. Han. *Spherical Harmonics and Approximations on the Unit Sphere: An Introduction*, volume 2044 of *Lecture Notes in Mathematics*. Springer, Berlin-Heidelberg, 2012.
- [3] A.V. Balakrishnan. Fractional powers of closed operators and the semigroups generated by them. *Pacific J. Math.* **10** (1960), 419–437.

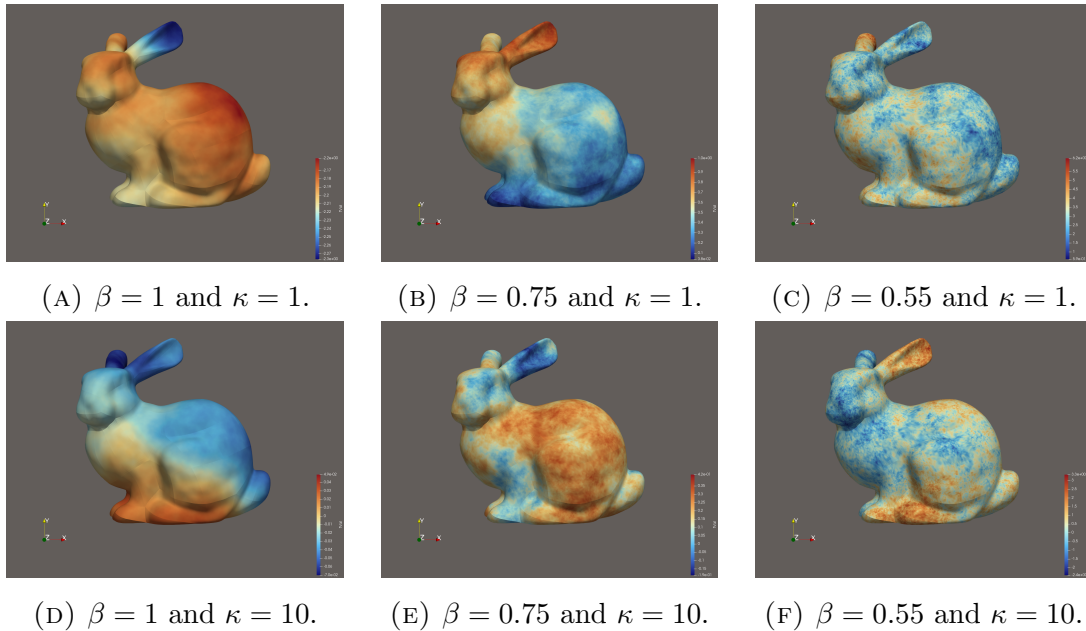


FIGURE 11. Whittle-Matérn Gaussian random fields on the Stanford bunny for different parameters of the fractional index β and the correlation length κ .

- [4] D. Bolin, K. Kirchner, and M. Kovács. Numerical solution of fractional elliptic stochastic PDEs with spatial white noise. *IMA J. Numer. Anal.* **40**(2) (2020), 1051–1073.
- [5] L. Beirão da Veiga, A. Buffa, G. Sangalli, and R. Vázquez. Mathematical analysis of variational isogeometric methods. *Acta Numer.* **23** (2014) 157–287.
- [6] A. Bonito, D. Guignard, and W. Lei. Numerical approximation of Gaussian random fields on closed surfaces. *Comput. Meth. Appl. Math.* **24**(4) (2024), 829–858.
- [7] A. Buffa, H. Harbrecht, A. Kunoth, and G. Sangalli. BPX-preconditioning for isogeometric analysis. *Comput. Meth. Appl. Math.* **265** (2013), 63–70.
- [8] J.A. Cottrell, T.J.R. Hughes, and Y. Bazilevs. *Isogeometric Analysis: Toward Integration of CAD and FEA*. Wiley, West Sussex, 2009.
- [9] J. Dölz, H. Harbrecht, S. Kurz, M. Multerer, S. Schöps, and F. Wolf. Bembel: Boundary element method based engineering library. <http://www.bembel.eu>.
- [10] J. Dölz, H. Harbrecht, S. Kurz, M. Multerer, S. Schöps, and F. Wolf. Bembel: The fast isogeometric boundary element C++ library for Laplace, Helmholtz, and electric wave equation. *SoftwareX* **11** (2020) 100476.
- [11] J. Dölz, H. Harbrecht, S. Kurz, S. Schöps, and F. Wolf. A fast isogeometric BEM for the three dimensional Laplace- and Helmholtz problems. *Comput. Methods Appl. Mech. Eng.* **330** (2018), 83–101.
- [12] A.A. Farag. *Biomedical Image Analysis: Statistical and Variational Methods*. Cambridge University Press, Cambridge, 2014.

- [13] N. Hale, N.J. Higham, and L.N. Trefethen. Computing \mathbf{A}^α , $\log(\mathbf{A})$, and related matrix functions by contour integrals. *SIAM J. Numer. Anal.* **46**(5) (2008), 2505–2523.
- [14] H. Harbrecht and M. Peters. Comparison of fast boundary element methods on parametric surfaces. *Comput. Methods Appl. Mech. Eng.* **261–262** (2013), 39–55.
- [15] H. Harbrecht, L. Herrmann, K. Kirchner, and Ch. Schwab. Multilevel approximation of Gaussian random fields: Covariance compression, estimation and spatial prediction. *Math. Mod. Meth. Appl. Sci.* **30**(1) (2020), 181–223.
- [16] L. Herrmann, K. Kirchner, and Ch. Schwab. Multilevel approximation of Gaussian random fields: fast simulation. *Math. Mod. Meth. Appl. Sci.* **30**(1) (2020), 181–223.
- [17] C. Hofreither and W. Zulehner. On full multigrid schemes for isogeometric analysis. In T. Dickopf et al., editors, *Domain Decomposition Methods in Science and Engineering XXII*, volume 104 of *Lect. Notes Comput. Sci. Eng.*, pp 267–274, Springer, Cham, 2016.
- [18] W. Huang and M. Multerer. Isogeometric analysis of diffusion problems on random surfaces. *Appl. Numer. Math.* **179** (2022), 50–65.
- [19] T.J.R. Hughes, J.A. Cottrell, and Y. Bazilevs. Isogeometric analysis: CAD, finite elements, NURBS, exact geometry and mesh refinement. *Comput. Methods Appl. Mech. Eng.* **194** (2005), 4135–4195.
- [20] E. Jansson, M. Kovács, and M. Pereira. Surface finite element approximation of spherical Whittle–Matérn Gaussian random fields. *SIAM J. Sci. Comput.* **44**(2) (2022) A825–A842.
- [21] E. Jansson, A. Lang, and M. Pereira. Non-stationary Gaussian random fields on hypersurfaces: Sampling and strong error analysis. arXiv-Preprint, arXiv:2406.08185 (2024).
- [22] A. Lang and Ch. Schwab. Isotropic Gaussian random fields on the sphere: regularity, fast simulation, and stochastic partial differential equations. *Ann. Appl. Probab.* **25**(6) (2015), 3047–3094.
- [23] F. Lindgren, H. Rue, and J. Lindström. An explicit link between Gaussian fields and Gaussian Markov random fields: the stochastic partial differential equation approach. *J. R. Stat. Soc. Ser. B Stat. Methodol.* **73** (2011), 423–498.
- [24] J. Lund and K.L. Bowers. *Sinc Methods for Quadrature and Differential Equations*. Society for Industrial and Applied Mathematics (SIAM), Philadelphia, PA, 1992.
- [25] B. Matérn. *Spatial Variation*, volume 36 of *Lecture Notes in Statistics*. Springer, Berlin, 2nd edition, 1986.
- [26] D. Marinucci and G. Peccati. *Random Fields on the Sphere. Representation, Limit Theorems and Cosmological Applications*, volume 389 of London Mathematical Society Lecture Note Series. Cambridge University Press, Cambridge, 2011.
- [27] L. Piegl and W. Tiller. *The NURBS Book*. Springer, Berlin-Heidelberg, 2nd edition, 1997.

- [28] N. Pietroni, E. Puppo, G. Marcias, R. Scopigno, and P. Cignoni. Tracing field-coherent quad layouts. *Computer Graphics Forum*, **35**(7) (2016), 485–496.
- [29] H. Rue and L. Held. *Gaussian Markov Random Fields. Theory and Applications*. Monographs on Statistics and Applied Probability, vol. 104, Chapman & Hall / CRC press, London, 2005.
- [30] C. Scarth, S. Adhikari, P.H. Cabral, G.H.C. Silva, and A. Pereira do Prado. Random field simulation over curved surfaces: Applications to computational structural mechanics. *Comput. Meth. Appl. Math.* **345** (2019), 283–301.
- [31] L.L. Schumaker. *Spline functions: Basic theory*. Cambridge Mathematical Library. Cambridge University Press, Cambridge, 2007.
- [32] E. Tong and Y. Lee. Marsden’s identity. *Comput. Aided Geom. Des.* **13**(4) (1996), 287–305.
- [33] P. Whittle. On stationary processes in the plane. *Biometrika* **41** (1954), 434–449.
- [34] P. Whittle. Stochastic processes in several dimensions. *Bull. Inst. Internat. Statist.* **40** (1963), 974–994.

HELMUT HARBRECHT, FLORIAN SONDEREGGER, REMO VON RICKENBACH, DEPARTMENT OF MATHEMATICS AND COMPUTER SCIENCE, UNIVERSITY OF BASEL, SPIEGELGASSE 1, 4051 BASEL, SWITZERLAND

Email address: {helmut.harbrecht,f.sonderegger,remo.vonrickenbach}@unibas.ch